TECHNICAL REPORT STANDARD TITLE PAGE

| 1. Report No. | 2. Government Accession No. | 3. Recipient's Catalog No. |
|---|---|---|
| FHWA/TX-83/7+256-3 | | |

| 4. Title and Subtitle | 5. Report Date |
|---|---|
| DETECTION OF CRACKS ON HIGHWAY PAVEMENTS | May 1983 |
| | 6. Performing Organization Code |

| 7. Author(s) | 8. Performing Organization Report No. |
|---|---|
| C. H. Chien, W. N. Martin, A. H. Meyer, and J. K. Aggarwal | Research Report 256-3 |

| 9. Performing Organization Name and Address | 10. Work Unit No. |
|---|---|
| Center for Transportation Research<br>The University of Texas at Austin<br>Austin, Texas 78712-1075 | 11. Contract or Grant No.<br>Research Study 3-8-80-256 |
| | 13. Type of Report and Period Covered |

| 12. Sponsoring Agency Name and Address | |
|---|---|
| Texas State Department of Highways and Public Transportation; Transportation Planning Division<br>P. O. Box 5051<br>Austin, Texas 78763 | Interim<br>14. Sponsoring Agency Code |

15. Supplementary Notes

Study conducted in cooperation with the U. S. Department of Transportation, Federal Highway Administration.
Research Study Title: "The Study of New Technologies for Pavement Evaluation"

16. Abstract

In a maintenance management program for continuously reinforced concrete pavement (CRCP), it is desirable to determine the rate of change of the crack spacing. When the crack spacing becomes smaller, than the designed spacing there is a potential for failure and therefore preventive maintenance may be considered. Since field measurement of crack spacings of highway pavements is impractical in areas with high traffic densities, image processing techniques using aerial photographs have been explored as a means for automating this process. Algorithms for detection of cracks of highway pavements in aerial photographs are presented in this report. In an aerial photograph of the pavement, edge points are identified and potential boundaries of water marks are labelled. Water marks can then be approximately located and crack spacing estimated.

| 17. Key Words | 18. Distribution Statement |
|---|---|
| water marks, crack spacings, Kirsch operator, non-maxima suppression, thresholding, Hough transform | No restrictions. This document is available to the public through the National Technical Information Service, Springfield, Virginia 22161. |

| 19. Security Classif. (of this report) | 20. Security Classif. (of this page) | 21. No. of Pages | 22. Price |
|---|---|---|---|
| Unclassified | Unclassified | 61 | |

Form DOT F 1700.7 (8-69)

# DETECTION OF CRACKS ON HIGHWAY PAVEMENTS

by

C. H. Chien
W. N. Martin
A. H. Meyer
J. K. Aggarwal

Research Report Number 256-3

The Study of New Technologies for
Pavement Evaluation

Research Project 3-8-80-256

conducted for

Texas State Department of Highways and
Public Transportation

in cooperation with the
U. S. Department of Transportation
Federal Highway Administration

by the

Center for Transportation Research
Bureau of Engineering Research
The University of Texas at Austin

May 1983

The contents of this report reflect the views of the authors, who are responsible for the facts and the accuracy of the data presented herein. The contents do not necessarily reflect the official views or policies of the Federal Highway Administration. This report does not constitute a standard, specification, or regulation.

## PREFACE

The authors are indebted to Mr. William V. Ward and the Houston Urban office for furnishing the aerial photographs used in this study. The authors wish to express a special thanks to the Laboratory for Image and Signal Analysis at The University of Texas at Austin which provided the equipment used in the analysis of the photographs.

C. H. Chien

W. N. Martin

A. H. Meyer

J. K. Aggarwal

## LIST OF REPORTS

Report No. 256-1, Comparison of the Falling Weight Deflectometer and the Dynaflect for Pavement Evaluation," by Bary Eagleson, Scott Heisey, W. Ronald Hudson, Alvin H. Meyer, and Kenneth H. Stokoe, presents the results of an analytical study undertaken to determine the best model for pavement evaluation using the criteria of cost, operational characteristics, and suitability.

Report No. 256-2, "Determination of In Situ Shear Wave Velocities From Spectral Analysis of Surface Waves," by J. Scott Heisey, Kenneth H. Stokoe II, W. Ronald Hudson, and A. H. Meyer, presents a method for determining elastic moduli at soil and pavement sites. Criteria considered in developing this method included the restraint of nondestructive testing, accuracy of moduli for all layers regardless of thickness, and quickness and effeciency for rapid, extensive testing.

Report No. 256-3, "Detection of Cracks on Highway Pavements," by C. H. Chien, W. N. Martin, A. H. Meyer, and J. K. Aggarwal, presents algorithms for the detection of cracks of highway pavements in aerial photographs.

ABSTRACT

In a maintenance management program for continuously reinforced concrete pavement (CRCP), it is desirable to determine the rate of change of the crack spacing. When the crack spacing becomes smaller, than the designed spacing there is a potential for failure and therefore preventive maintenance may be considered. Since field measurement of crack spacings of highway pavements is impractical in areas with high traffic densities, image processing techniques using aerial photographs have been explored as a means for automating this process. Algorithms for detection of cracks of highway pavements in aerial photographs are presented in this report. In an aerial photograph of the pavement, edge points are identified and potential boundaries of water marks are labelled. Water marks can then be approximately located and crack spacing estimated.

KEY WORDS: Water marks, crack spacings, Kirsch operator, non-maxima suppression, thresholding, Hough transform.

## SUMMARY

Since field measurement of crack spacings of highway pavements is impractical in areas with high traffic densities, image processing of aerial photographs is proposed and explored as a means of automating such measurement. Crack widths range from 0.01 to 0.02 inches and thus are too small to be detected in the digitized pictures of aerial photographs taken at heights above 1000 feet at the resolution commonly used for pictures (e.g., 256 - 1024 pixels [picture elements] on each side). However, if a picture of a highway pavement is taken immediately after it has rained, water marks which form around the cracks can be seen. It is reasonable to assume that one crack is associated with each water mark, and, therefore, in this procedure water marks are used for estimating crack spacings.

The approach consists of, first, locating the water marks, by detecting the boundaries of the water marks. The edges corresponding to region boundaries in photographs may be detected by using one of many available edge operators, e.g., the Laplacian operator, the Kirsch operator, etc. Use is then made of an edge operator coupled with a non-maxima suppression technique to reduce noise. The resulting boundaries of the water marks are used to guide the search for crack locations and to estimate crack spacings.

This report is organized as follows. Chapter 1 is an introduction to the subject, Chapter 2 contains a description of the edge detection procedure, which is used to extract the edge points from the picture of the

highway pavement and essentially consists of three steps: (1) gradient computation, (2) non-maxima suppression, and (3) thresholding. Intensity gradients are computed by applying the Kirsch operator to the intensity picture. This step yields a gradient picture. The non-maxima suppression step selects only those pixels at which the gradient values are local maxima. This step is crucial because the Kirsch operator results in a cluster of high responses around the positions of true edges. Finally, thresholding deletes those pixels at which the gradient values are less than some threshold. A binary edge picture is obtained after thresholding. In Chapter 3, a modified version of the Hough transform technique is described and applied to the binary edge picture to find the direction of the road and road sections. Algorithms are developed in Chapter 4 to describe how water marks are detected and how crack spacings are estimated. The evaluation of these algorithms is presented in Chapter 5. Some future directions of the research related to the techniques for the evaluation of the conditions of highway pavements are briefly mentioned in Chapter 6.

Due to the high cost of analysis (about $600 per mile of pavement for computer time alone) and the requirement of a photograph of a recently wetted pavement, the method is not practically applicable at the present time.

## IMPLEMENTATION STATEMENT

The report provides a sound foundation for work in applying computer enhancement techniques to the analysis of aerial photographs. However the high cost of analysis and the requirement of a photograph of a wetted pavement render the method unimplementable at the present time.

TABLE OF CONTENTS

# CHAPTER 1. INTRODUCTION

## PROBLEM DESCRIPTION

The objective of this study is to locate cracks and measure crack spacings using aerial photographs of highway pavements. The pavement investigated is a continuously reinforced concrete pavement (CRCP) section in the Houston area. CRCP is designed to crack at intervals of 4 to 8 feet. The design eliminates the need for transverse joints. Experience has shown that, as the pavement deteriorates with time, new cracks form and hence the crack spacing becomes smaller. In a maintenance management program it is desirable to determine the rate of change of the crack spacing and to identify those areas where the crack spacing has become small enough to indicate a potential failure in the pavement and thus a need for preventive maintenance.

## SOME DIFFICULTIES

The physical widths of cracks are on the order of 0.01 to 0.02 inches (Ref 1). The resolution of the digitized pictures from aerial photographs taken above 1000 feet is insufficient to resolve such minute detail. However, after it has rained, water marks form around the cracks. They are comparatively much larger and distinguishable from the pavement. It is

reasonable to assume that there is usually one crack associated with each water mark. Therefore, the relative density of water marks and spacings of adjacent water marks are measured, and the crack spacings estimated. Water marks are not easy to detect for the following reasons:

(1) If two or more cracks are close to each other, the water marks surrounding them will merge into one and become indistinguishable.

(2) There are no well-defined boundaries for water marks because water marks are products of the infiltration phenomenon.

(3) There are usually road film stripes in the center of the lanes which cover water marks and make them more difficult to detect.

With these difficulties, it is impossible to detect exactly the individual water marks. However, (1) the pixels (picture elements) in the neighborhood of the boundaries of water marks usually have locally higher gradient values, and (2), on CRC pavements, most cracks are in a direction transverse to the road. These two observations suggest that the number (or the density) of edge points corresponding to a water mark will be a good indicator of its location. An edge point corresponding to a water mark is defined here as a pixel with high intensity gradient value in a direction nearly parallel to the direction of the road.

## SYSTEM DESCRIPTION

The system to detect cracks on a highway pavement from an aerial photographs includes four procedures:

(1) Picture digitization. A video camera and a digitizer are used to digitize an aerial photograph. This procedure is necessary for image processing and is not described in this report.

(2) Edge detection. This procedure detects the edges at the boundaries of the road and water marks. The Kirsch operator (Ref 2), a non-maxima suppression technique (Ref 3) and thresholding are used in the procedure to find these edges. The Kirsch operator is applied to the intensity picture to compute the gradient at each pixel. Non-maxima suppression deletes those pixels at which the gradient values are not local maxima. The output of the non-maxima suppression procedure (called a non-maxima suppressed picture) contains the edge points at the boundaries of the road, at the sawed joints between lanes, and in the neighborhood of the boundaries of water marks. This picture will be used in procedure 4. For detecting road sections and the direction of the road, the edge points with gradient values less than some threshold are deleted, since the gradient values at the points on the boundaries of the road and at the sawed joints are generally higher than those in the neighborhood of the boundaries of water marks, and the latter are not needed in the road detection procedure.

(3) Road detection. With the edge points selected in procedure 2, the lines corresponding to the margins of the road and the saw joints between lanes can be extracted using a line detection technique, a modified version of the Hough transform (Ref 4). Thus, the margins of the road and road sections can be found.

(4) Labelling of potential edge lines and potential boundaries. After locating the margins of the road and finding the road sections in procedure 3, we are ready to locate water marks. The non-maxima suppressed picture obtained in procedure 2 is used in this procedure. "Potential edge lines" are labelled according to the number of edge points (corresponding to water marks) related to line segments orthogonal to the direction of the road. Non-maxima suppression based on the number of edge points (also corresponding to water marks) is used to label "potential boundaries." Hence water marks and cracks can be located, and crack spacings calculated.

The flow chart of this system is depicted in Fig 1.1. Except for the picture digitization, the other procedures will be discussed in the remainder of this report which is organized as follows.

Chapter 2 contains a description of the edge detection procedure. This procedure contains basically three steps: (1) gradient computation using the Kirsch operator, (2) non-maxima suppression, and (3) thresholding. In Chapter 3, a modified version of the Hough transform technique is described and applied to the thresholded picture to find the direction of the road and

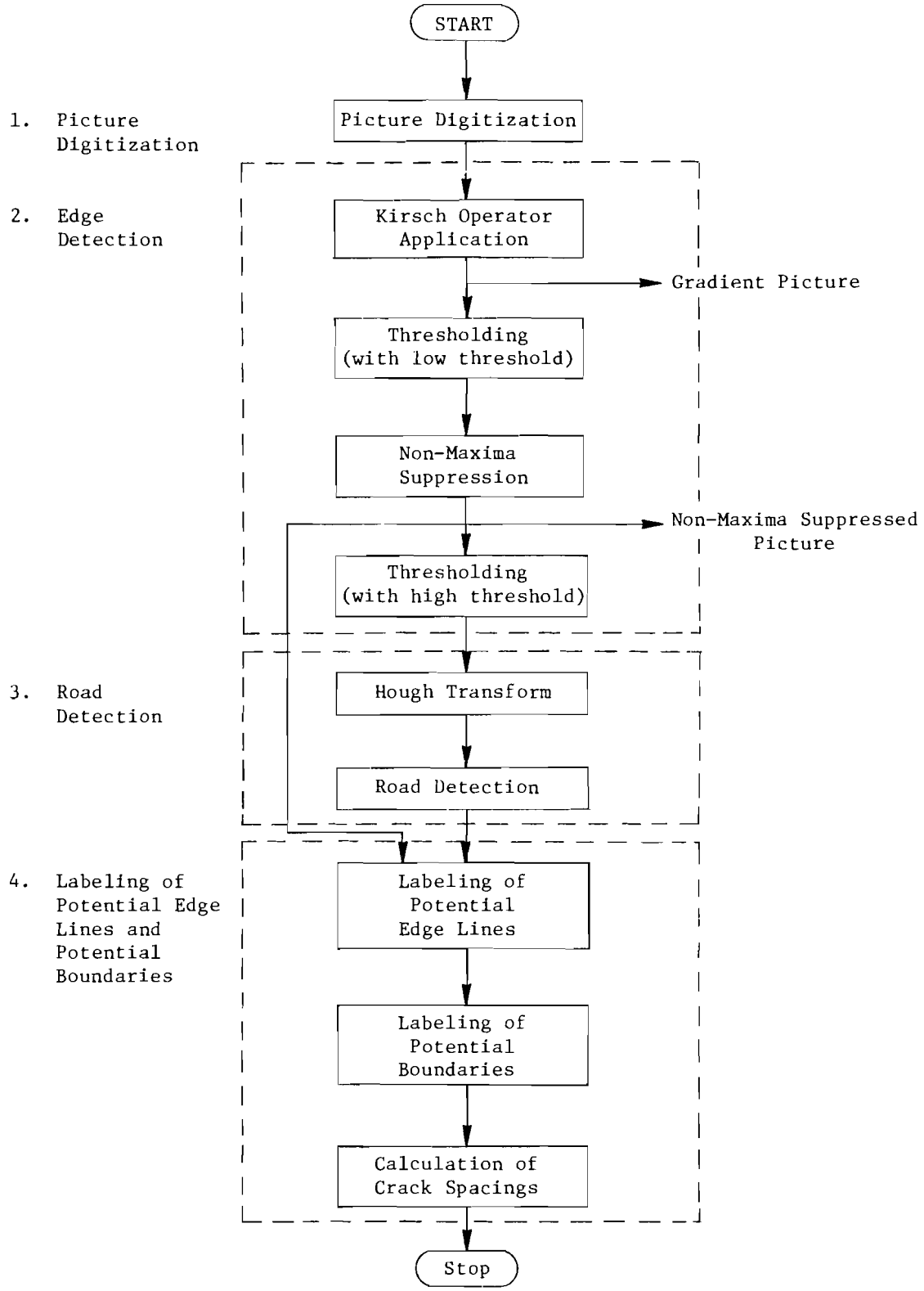


Fig 1.1. Flow chart of the system to detect cracks on a highway pavement.

road sections. Algorithms are developed in Chapter 4 to detect water marks and measure crack spacings. The evaluation of these algorithms is presented in Chapter 5. Some future directions of the research related to the techniques for the evaluation of the conditions of highway pavements are briefly mentioned in Chapter 6.

# CHAPTER 2. EDGE DETECTION

The edge detection procedure used to extract edges from the picture of a highway pavement consists of essentially three steps: (1) gradient computation, (2) non-maxima suppression, and (3) thresholding. Intensity gradients are computed by the application of the Kirsch operator to the intensity picture. This step yields a gradient picture. The non-maxima suppression step will select only those pixels at which the gradient values are local maxima. This step is crucial because the Kirsch operator results in a cluster of high responses around the positions of true edges. Finally, thresholding deletes the pixels whose gradient values are less than some threshold.

## THE KIRSCH OPERATOR

There are a variety of edge operators reported in the literature. Examples are the Laplacian operator (Ref 5), the Roberts operator (Ref 6), the Sobel operator (Ref 7), the Kirsch operator, and others proposed by Prewitt (Ref 8), Argyle (Ref 9), Macleod (Ref 10), and Rosenfeld (Ref 11).

The Kirsch operator (Ref 2) is a nonlinear edge operator introduced by Kirsch which calculates the intensity gradient for each of eight directions centralled at the pixel P(I,J) (see Fig 2.1) and chooses the maximum of

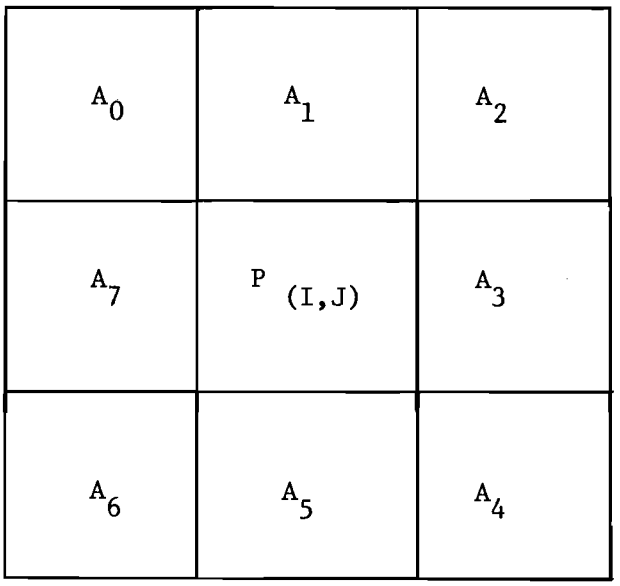


Fig 2.1. Numbering for 3 x 3 Kirsch Operator.

those values as the gradient value of the central pixel. The corresponding direction is defined as the direction of the gradient. Basically, the Kirsch operator provides the maximal compass gradient value about a pixel (Ref 12).

Referring to Fig 2.1, the gradient value, G , at the pixel P(I,J) is given by

$$G(I,J) = MAX\left\{ 1, MAX \left[ S_k/3 - T_k/5,\ 0 \leq k \leq 7 \right] \right\} \qquad (2.1)$$

where

$$S_k = A_k + A_{k+1} + A_{k+2}$$

$$T_k = A_{k+3} + A_{k+4} + A_{k+5} + A_{k+6} + A_{k+7}$$

$A_{k+m}$ where $(0 \leq m \leq 7)$ are the intensities of the pixels in the 3 x 3 neighborhood of the pixel P(I,J), and the subscripts of the A are evaluated modulo 8.

Shown in Fig 2.2 through Fig 2.5 are two road pictures and the results of applying the Kirsch operator to these two pictures. Observe the clusters of edge points in Fig 2.3 and Fig 2.5. The clustered regions can be thinned using a non-maxima suppression technique based on the intensity gradient, which is introduced in the following section.

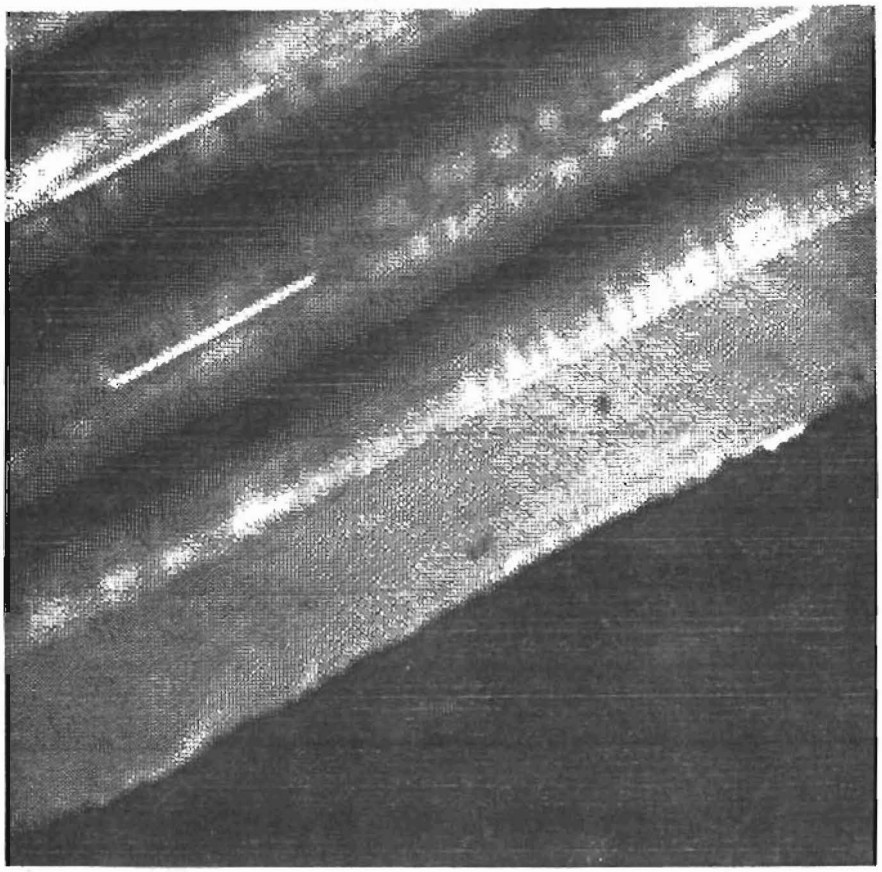

Fig 2.2. Digitized picture of a highway pavement (Hwy 1).

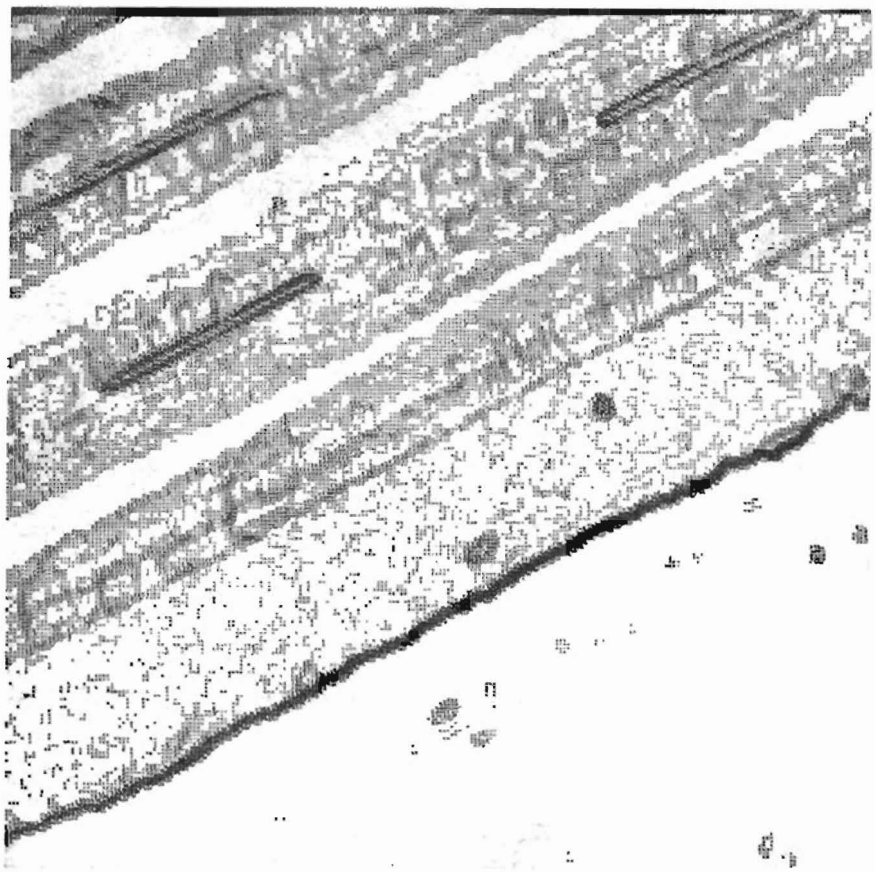

Fig 2.3. Gradient picture of Fig 2.2.

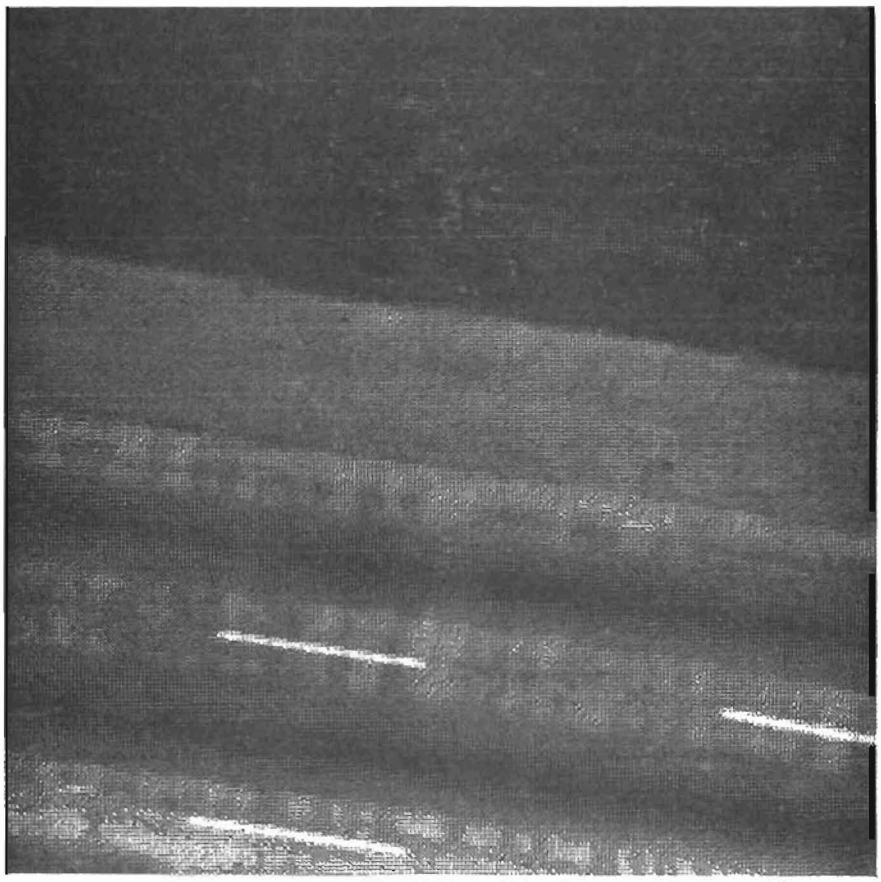

Fig 2.4. Digitized picture of a highway pavement (Hwy 2).

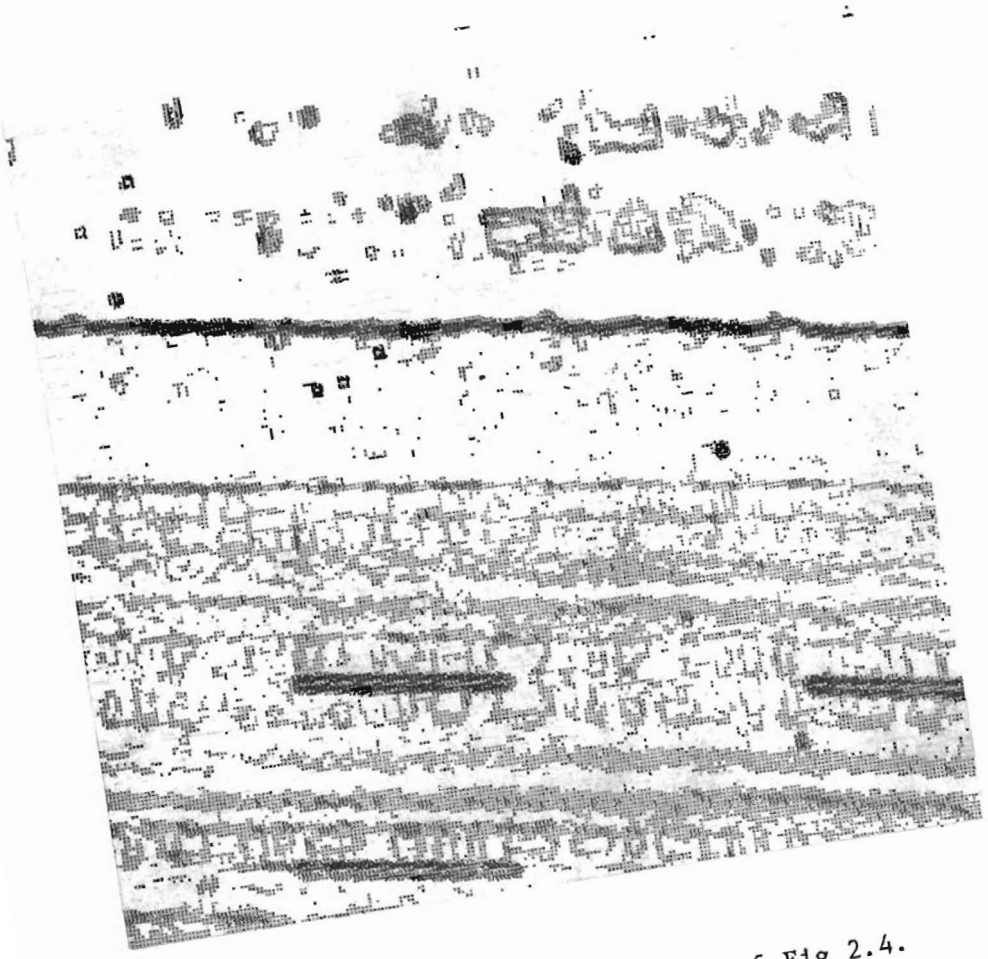

Fig 2.5. Gradient picture of Fig 2.4.

## NON-MAXIMA SUPPRESSION

There is a necessity for the non-maxima suppression procedure because there is no well-defined boundary for a water mark. If the water mark is several pixels wide, then those pixels interior to the water mark should not be labelled as edge points. In order to eliminate most of the edge responses of the points in the interior of water marks, the non-maxima suppression (Ref 3) was performed on the gradient picture based on the intensity gradient (Ref 13).

An edge orientation $\overline{E}$ and a gradient values G are associated with each pixel in the gradient picture. Passing through each point is a line segment orthogonal to edge orientation E at this point (see Fig 2.6). All edges on this line segment whose gradient values are less than G are deleted. Figure 2.7 shows the result of non-maxima suppression of the gradient picture in Fig 2.5.

## THRESHOLDING

Since the direction of the road is desired, and most of the edge points on road film strips or sawed joints have high contrast, it is possible to apply a modified version of the Hough transform (a line and curve detection technique) to only those pixels with gradient values greater than the threshold $T_{g_2}$ . The threshold is calculated from Eq 2.2:

$$T^2_{g_2} = \frac{\sum_{G=0}^{255} H(G)*G^2}{\sum_{G=0}^{255} H(G)} = \sum_{G=0}^{255} P(G)*G^2 \qquad (2.2)$$

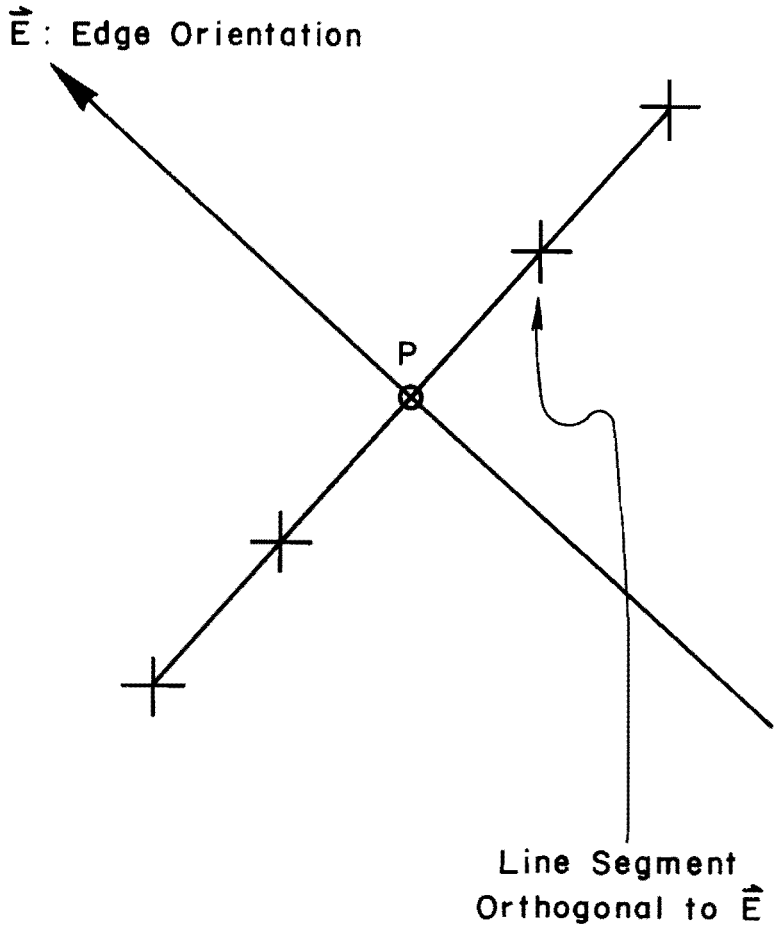


Fig 2.6. Operation of non-maxima suppression.

Fig 2.7. Non-maxima suppressed picture of Fig 2.5.

where

$$P(G) = \frac{H(G)}{\sum_{G=0}^{255} H(G)}$$

H(G) is the number of pixels with the gradient value G , and P(G) is the relative frequency associated with H(G). Actually, $T_{g_2}$ is the square root of the second moment of the gradient values.

The number of points on which the Hough transform is performed should be small, for computational efficiency. Using the second moment of the gradient values as a threshold will produce less points in the thresholded picture than using the mean of the gradient values. This is the reason for not taking the mean of the gradient values as a threshold.

The result of applying non-maxima suppression and thresholding to the gradient picture in Fig 2.5 is shown in Fig 2.8.

Actually, thresholding was applied twice in this study; once on the gradient picture, with low threshold $T_{g_1}$ , which is half of the mean of the gradient values, and the other time (with high threshold $T_{g_2}$ ) on the edge picture obtained after performing the non-maxima suppression procedure. Since non-maxima suppression requires more computational time than thresholding, it is advantageous to perform thresholding first. The problem is that the contrast of the pixels around the boundaries of water marks is lower than that at the boundaries of road sections. If the threshold value is too high, most edge points around the boundaries of water marks will be suppressed. On the other hand, with low threshold value, performing the

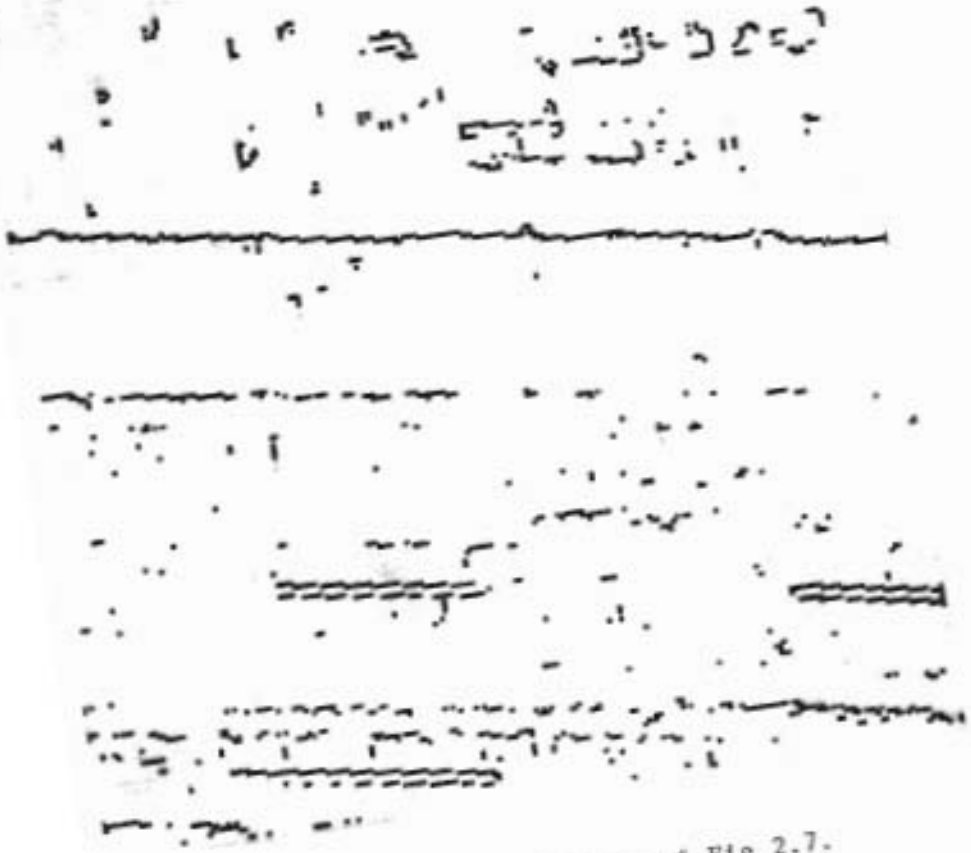

Fig 2.8. Binary picture of Fig 2.7.

Hough transform would be computationally expensive. This suggests applying thresholding twice with different threshold values as needed.

# CHAPTER 3. DETECTION OF ROAD SECTIONS

## THE HOUGH TRANSFORM

The Hough transform (Ref 14), developed by Hough, involves the transformation of a line in the Cartesian coordinate plane X-Y to a point in the polar coordinate plane $\rho - \theta$, as shown in Fig 3.1. Let O be the origin of the Cartesian coordinate plane, L be an arbitrary line, and $\overline{OP}$ be the line segment orthogonal to the line L ; then the line L may be parametrically described by the equation

$$\rho = \overline{OP} = x\text{COS}\theta + y\text{SIN}\theta \qquad (3.1)$$

where $\rho$ is the length of the line segment $\overline{OP}$, and O is the angle $\overline{OP}$ makes with the X-axis.

The family of lines in Fig 3.2 passing through a common point P maps into a curve in the $\rho - \theta$ domain as shown in Fig 3.2. The three curves in the $\rho - \theta$ domain which correspond to the three families of straight lines passing through collinear points A, B, and C in the X-Y domain cross at a single point ( $\rho_o$, $\theta_o$ ), as depicted in Fig 3.3.

Duda and Hart (Ref 4) have adapted the Hough transform technique to detect lines and curves in digital pictures. Each discrete data point in the

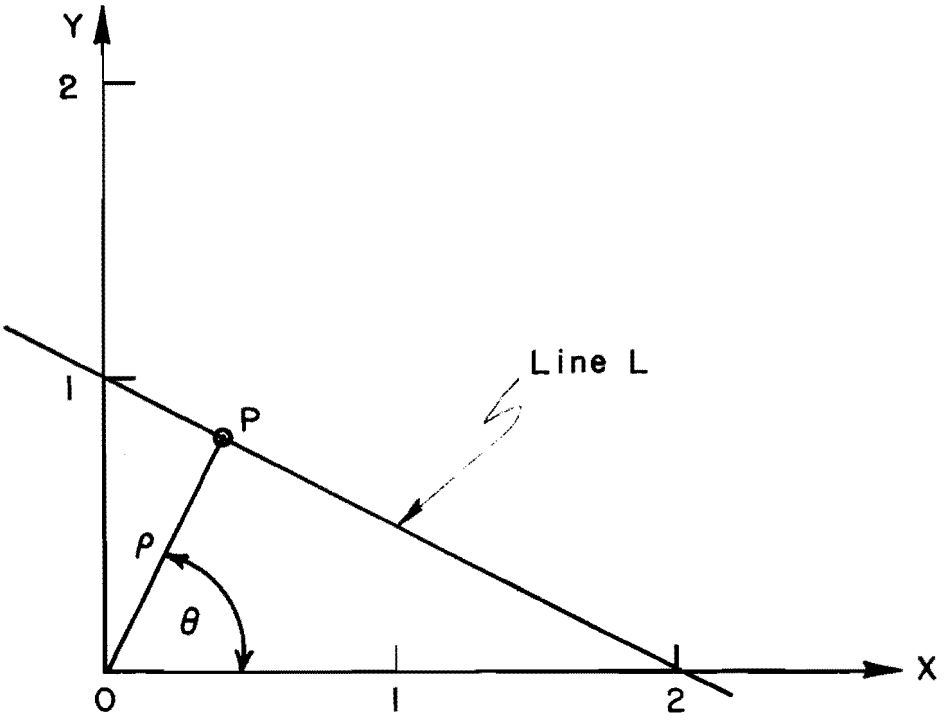


(a) Parametric line.

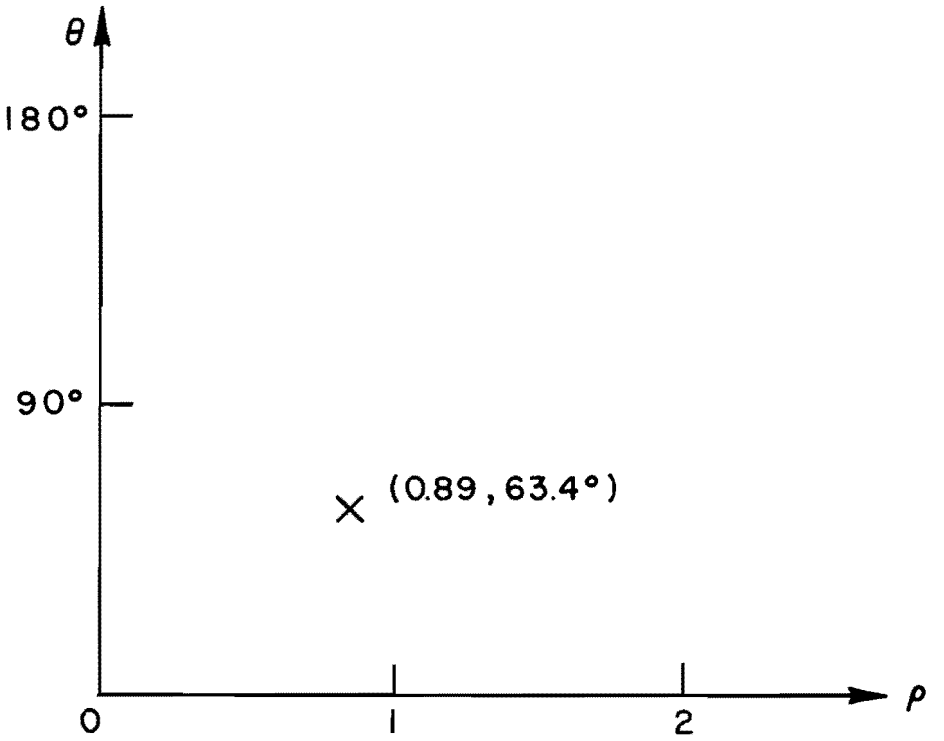


(b) Hough transform of (a).

Fig 3.1. Hough transform of a line.

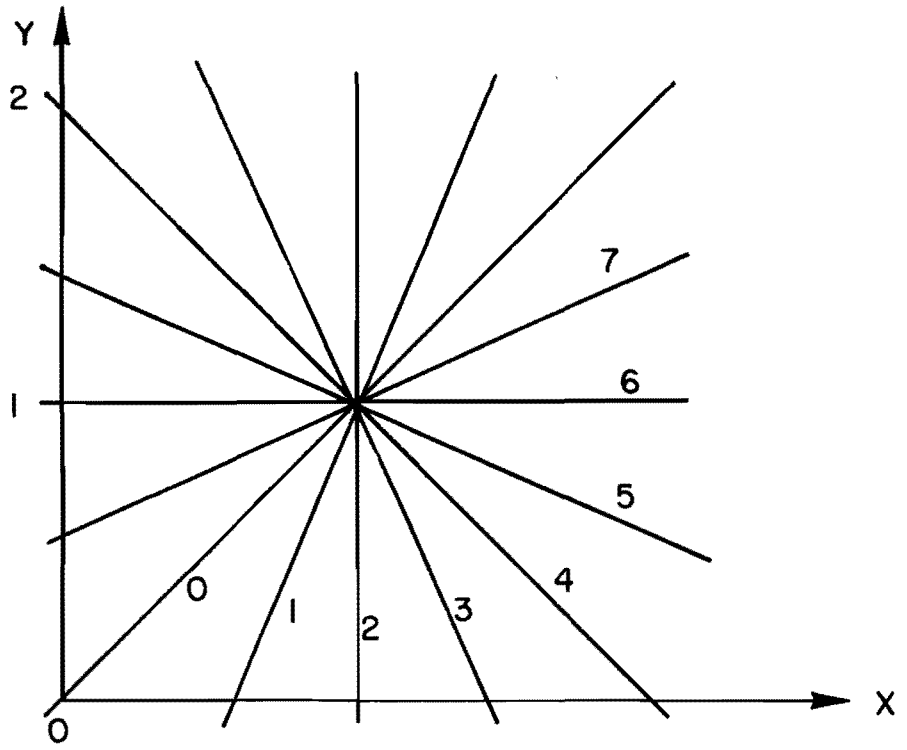


(a) Family of lines passing through a common point P.

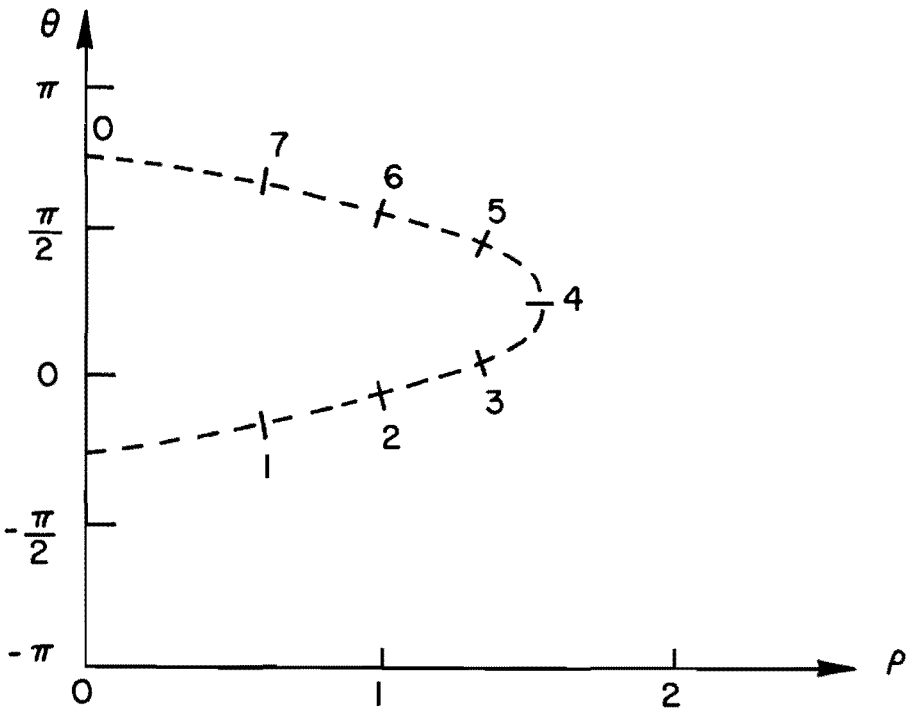


(b) Hough transform of (a).

Fig 3.2. Hough transform of a family of lines.

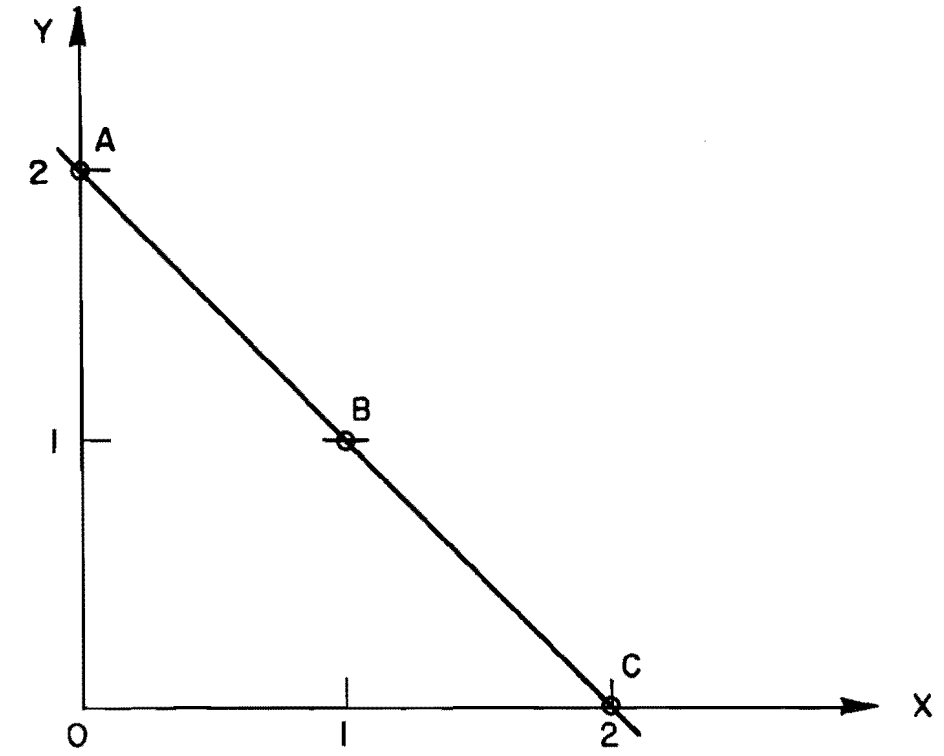


(a) Collinear points A, B, C.

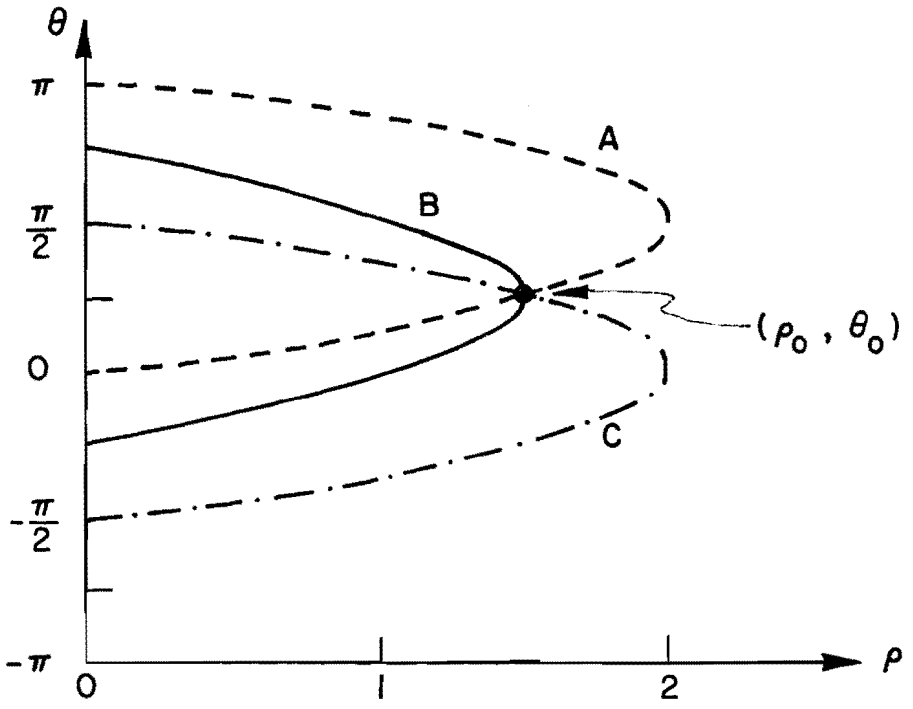


(b) Hough transform of (a).

Fig 3.3. Hough transform of collinear points.

X-Y domain is transformed to a curve in the $\rho - \theta$ domain which is quantized into an array of accumulators. The basic algorithm for the Hough transform is as follows:

(1) Quantize the parameter space $\rho - \theta$ with appropriate $\Delta\rho$ and $\Delta\theta$ in the range of the maximal and minimal values for $\theta$ and 0 .

(2) Form an accumulator array $A(\rho, \theta)$. All the entries in this array are initialized to zero.

(3) Performing the following step: For each non-zero data point $P(x_i, y_i)$ do

For $\theta_j := 0°$ to $179°$ step $\Delta\theta$ do

Begin $\rho_{i_j}$ INT $(x_i \text{COS}\theta_j + y_i \text{SIN}\theta_j)$;

$A(\rho_{i_j}, \theta_j)$ $A(\rho_{i_j}, \theta_j) + 1$; END

Each entry $(\rho_i, \theta_j)$ in the accumulator array corresponds to the number of the points on the line with $\rho$ equal to $\rho_i$ and 0 equal to $\theta_j$ . The entry with the largest value corresponds to the line with the largest number of points on it in the binary picture.

In this study, 0 was 5° and $\Delta\rho$ was 1, 2, or 4 for different cases (this is discussed in more detail later).

More than one straight line needs to be extracted for the determination of the direction of the road; this suggests the use of the procedure described by Fennama and Thompson (Ref 15), who used the Hough transform to find the velocities for different objects in the picture. The parameters they used were $|V|$ and $\theta_v$ , which were the magnitude and the angle of the velocity and were related by the equation

$$|V| = \frac{\Delta I}{|G| \text{COS}\ (\theta_G - \theta_v)} \tag{3.2}$$

where $|G|$ and $\theta_G$ were the magnitude and the angle of the gradient, and $\Delta I$ was the intensity difference between two successive frames. All these three parameters were related to each data point and could be measured from the sequence of pictures. When the Hough transform was applied to all the data points in the picture, a peak in the accumulator array was found and the corresponding $(|V|, \theta_V)$ was assigned to those pixels satisfying the relation represented by Eq 3.2. Since more than one object having distinct velocities were to be located, the analysis was repeated using the data points of the original picture minus those data points already assigned a velocity. This procedure continued until no sufficiently well defined peaks were found in the accumulator array.

For the photographs used, the procedure described above is inefficient for detecting a large number of straight lines for determining the direction of the road, since performing the Hough transform requires a large amount of computation. We applied the Hough transform only once to each picture for two reasons: (1) the direction of the road is determined as the direction that occurs most often, and, thus, the number of lines to be detected should be large enough and be detected in one pass for efficiency; and (2) the only difference between Fennama's approach and the one used is whether the point at the intersection of straight lines should be assigned to only one line or to more than one line. (In this case, the intersecting point is assigned to all the straight lines passing through it.) Since the number of points on the lines to be detected is on the order of 100, there is little effect on the order in which the lines are detected. Therefore, this will not affect the determination of the direction of the road.

QUANTIZATION ERROR

Another problem is with the quantization error. In the continuous case, all the collinear points are mapped into the same entry in the accumulator array. For the discrete case, this is not always true. If the direction of the straight line is not exactly equal to a multiple of 5°, the points on it will be mapped into several entries. The analysis of the quantization error for this case is described below (see Fig 3.4).

Let

-L = be a straight line in the direction $\theta + 90°$,

-$\theta_j$ = be the quantized value nearest to $\theta$ ,

-Q = be an arbitrary (data) point on the line L,

-L' = be the line passing through Q with the direction $\theta_j + 90°$,

-$\overline{OP}$ = be the line segment passing through the origin O and orthogonal to L' at P, and

-$\rho_i$ = be the length of $\overline{OP}$ , and $\rho_1$ and $\rho_2$ be the minimal and maximal value of $\overline{OP}$ .

Then

$$0 \leq | \theta - \theta_j | = \Delta \theta \leq 2.5° \qquad (3.3)$$

and

$$\text{MAX } (\rho_2 - \rho_1) = \left( \frac{Y_s}{\text{SIN}\theta} \right) * \text{SIN } 2.5° \qquad (3.4)$$

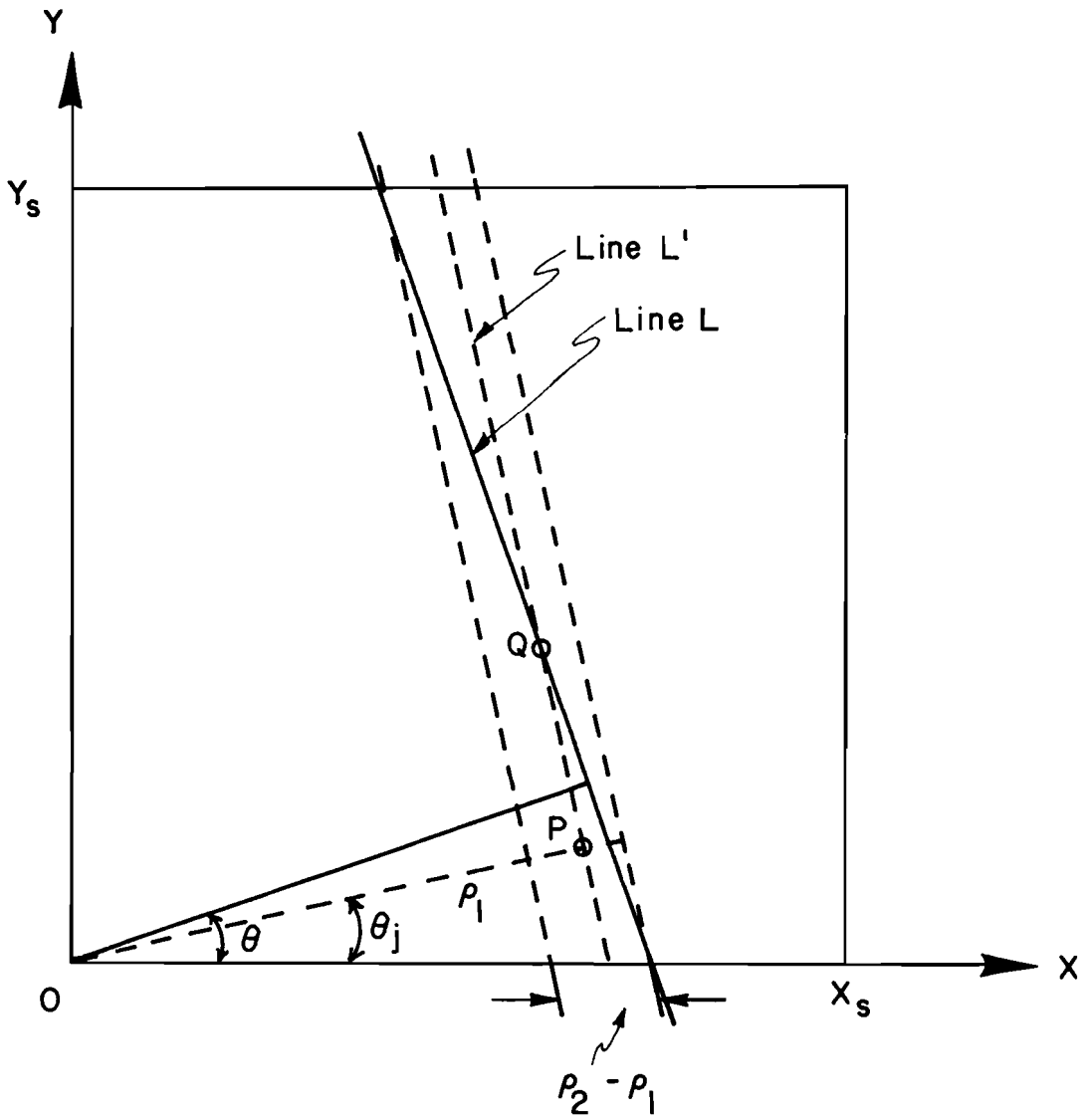


Fig 3.4. Due to quantization of $\Theta_j$, collinear points on the line L fall into different accumulators $(\rho_i, \Theta_j)$, where $\rho_1 \leq \rho_i \leq \rho_2$.

If

$$45° < 135° \quad \text{then}$$

$$\text{MAX } (\rho_2 - \rho_1) = 2 * Y_s * \text{SIN } 2.5° = 13.82$$

where $Y_s$ is the number of lines of the digital picture and is equal to 224 in this study.

For the worst case, the points on the line L will be mapped into 24 different entries with the same $\theta_j$ and different $\rho_i$. Suppose that 0 is equal to 45.24° and the total number of the data points on the line L is equal to N, then

$$\rho_2 - \rho_1 = 12.154$$

The points on the line L are mapped into different entries $A(\rho, 45)s$,

$$\rho = \rho_1 + K \quad ( 0 \leq K < 13 )$$

and $\rho_1$ is assumed to be an integer. Thus the values of all these $A(\rho, 45)s$ are about N/13 instead of N. It is possible that most of the lines detected are in the direction exactly equal to some multiple of 5°, and the direction of the road will not be determined correctly. Therefore, two modifications are needed for applying the Hough transform to find the direction of the road. First, a large $\Delta\rho$ is used to sample edge points from the binary picture. Second, for each increment of accumulators

$A(\rho_i, \theta_j)$, both $A(\rho_{i-1}, \theta_j)$ and $A(\rho_{i-1}, \theta_j)$ are incremented at the same time.

The results of applying the Hough transform with different sampling distances to the pictures of Figs 2.2 and 2.4 are listed in Table 3.1.

There is another benefit from larger sampling distances. The computational time for the Hough transform is proportional to the number of edge points to be transformed. Note in Table 3.1 that the number of edge points decreases as the sampling distance increases. The same is true for computational time. The number of edge points can also be decreased by using a high threshold when the binary picture is created. However, as the aerial photograph may be non-uniformly illuminated, some edge points (at the sawed joints) may not be detected using a high threshold, and road sections will not be determined correctly.

## DETECTION OF ROAD SECTIONS

Choose 25 accumulators with large values from the array of accumulators and the direction of the road can be obtained from the direction $\theta_m$ corresponding to the maximal entry in the array of accumulators. Since $\theta_m$ is the angle between the line segment $\overline{OP}$, which passes through the origin and is orthogonal to the direction of the road (see Fig 3.1a), and the relationship between the direction of the road E and $\theta_m$ is expressed by the equation

$$E = (\theta_m + 90°) \bmod 180° \tag{3.5}$$

TABLE 3.1. ACTUAL AND ESTIMATED DIRECTIONS OF ROAD

(a) FROM FIG 2.2

| | $N_s$ | W | $N_e$ | Direction |
|---|---|---|---|---|
| Actual | X | X | XXXX | 25° |
| HT-1 | 1 | 1 | 3591 | 0° |
| HT-2 | 2 | 1 | 908 | 0° |
| HT-3 | 4 | 1 | 228 | 25° |
| HT-4 | 1 | 3 | 3591 | 30° |
| HT-5 | 2 | 3 | 908 | 25° |
| HT-6 | 4 | 3 | 228 | 25° |

(b) FROM FIG 2.4

| | $N_s$ | W | $N_e$ | Direction |
|---|---|---|---|---|
| Actual | X | X | XXXX | 170° |
| HT-1 | 1 | 1 | 1441 | 170° |
| HT-2 | 2 | 1 | 362 | 0° |
| HT-3 | 4 | 1 | 90 | 170° |
| HT-4 | 1 | 3 | 1441 | 170° |
| HT-5 | 2 | 3 | 362 | 170° |
| HT-6 | 4 | 3 | 90 | 170° |

$N_s$ = the sampling distance

$N_e$ = the number of edge points to be transformed

W = the number of accumulators to be incremented concurrently

Having determined the direction of the road $E$, all the straight lines in this direction are sorted in ascending order. Let the minimal distance $D_m$ be the threshold for finding the lanes of the road ($D_m$ is about one third the width of the lane), and check the distance between two adjacent lines (also in ascending order). The first occurrence of the line separated from the next adjacent line by a distance larger than $D_m$ is labelled as the left margin of the road. The last occurrence of the line separated from a previous adjacent line by a distance larger than $D_m$ is labelled as the right margin of the road.

After locating the margins of the road, we are ready to find the sawed joints along the road. Since the lines with direction $E$ are edges of road film stripes or sawed joints, and the intensities of the road film stripes are usually lower than those of the sawed joints, the average intensity for each line in the direction of the road can be used to distinguish road film stripes from sawed joints.

# CHAPTER 4. ALGORITHMS FOR LOCATING CRACKS

In this chapter, algorithms to measure the relative densities and locations of water marks and estimate crack spacings are described. The detection of road sections has been described in Chapter 3. It is now possible to restrict our observation to road sections only. The algorithms described here are based on the assumption that there are no cars on the road. If there are cars on the road, it is necessary to identify the cars first. In general, a car on the highway is separated from other cars (on the same lane) by at least 50 feet and the road in the picture ranges about 50 feet in length. Therefore, there is at most one car in each lane and the crack spacing estimated by these algorithms will reflect the actual condition of the pavement without significant error. A technique for the detection of cars on the road can be found in reference 16 and is not considered here.

## OVERVIEW OF ALGORITHMS

In order to detect water marks and locate cracks, it is necessary to extract edges at the boundaries of water marks. As mentioned earlier, the water marks on the highway pavement are in the direction nearly orthogonal to that of the road. An edge point is defined as a pixel with a local maximal intensity gradient value and with the direction of the gradient approximately

parallel to that of the road. After extracting edge points, "potential edge lines" are labelled according to the number of edge points related to the line segments orthogonal to the direction of the road. With the "potential edge lines", non-maxima suppression based on the number of edge points is used to label "potential boundaries." Finally, water marks and cracks can be located and crack spacings calculated.

The procedure for locating water marks and cracks can be divided in two steps:

(1) Labelling of "potential edge lines" and calculating the densities of water marks in different regions based on the number of "potential edge lines" in those regions.

(2) Labelling of "potential boundaries" using non-maxima suppression based on the number of edge points on the "potential edge lines." Locate water marks and cracks.

## POTENTIAL EDGE LINES

For CRC pavements, most cracks and water marks lie in a direction nearly orthogonal to the direction of the road. Although the boundaries of water marks cannot be exactly located (for their boundaries are not well-defined), the number (or the densities) of edge points corresponding to water marks are a good indicator of their locations. Potential edge lines are labelled according to the following steps:

(1) Divide the pavement into regions associated with the lanes of the road.

(2) Divide each lane into subregions. (An 8-pixel-wide subregion seems adequate and is used in this study.)

(3) For each possible line segment in the subregion that is orthogonal to the direction of the road, count the total number of edge points on this line segment and both of its adjacent line segments. Only

edge points with a direction nearly orthogonal to that of the road are counted.

(4) If the total number of edge points counted is greater than a threshold , the corresponding line segment is labelled as a "potential edge line."

(5) For each subregion, count the number of potential edge lines in it. Find a threshold $T_1$ by taking the simple average of all these numbers.

(6) Compare the number of potential edge lines of each subregion with the threshold $T_1$ . The region with the number of potential edge lines higher than the threshold $T_n$ is labelled as a region with high density of water marks (otherwise, low density). If more than one subregion are labelled as high density and they are next to each other, merge them into one region.

This algorithm can also be used to compare the density of water marks on two sections of the highway pavement, if these two sections have been normalized to the same size. Figures 4.1 through 4.4 show two road pictures and the corresponding modified pictures with frames surrounding the regions with high density of water marks. It can be seen that there are more water marks on the road section in Fig 4.1 than the road section in Fig 4.3.

## POTENTIAL BOUNDARIES

With potential edge lines labelled in the previous algorithm, non-maxima suppression based on the number of edge points on the potential edge lines is used to approximately locate the boundaries of water marks and locations of cracks. Crack spacings can be subsequently estimated. Potential boundaries are labelled according to the following steps:

(1) Label the potential edge lines using step 1 through step 4 of the previous algorithm.

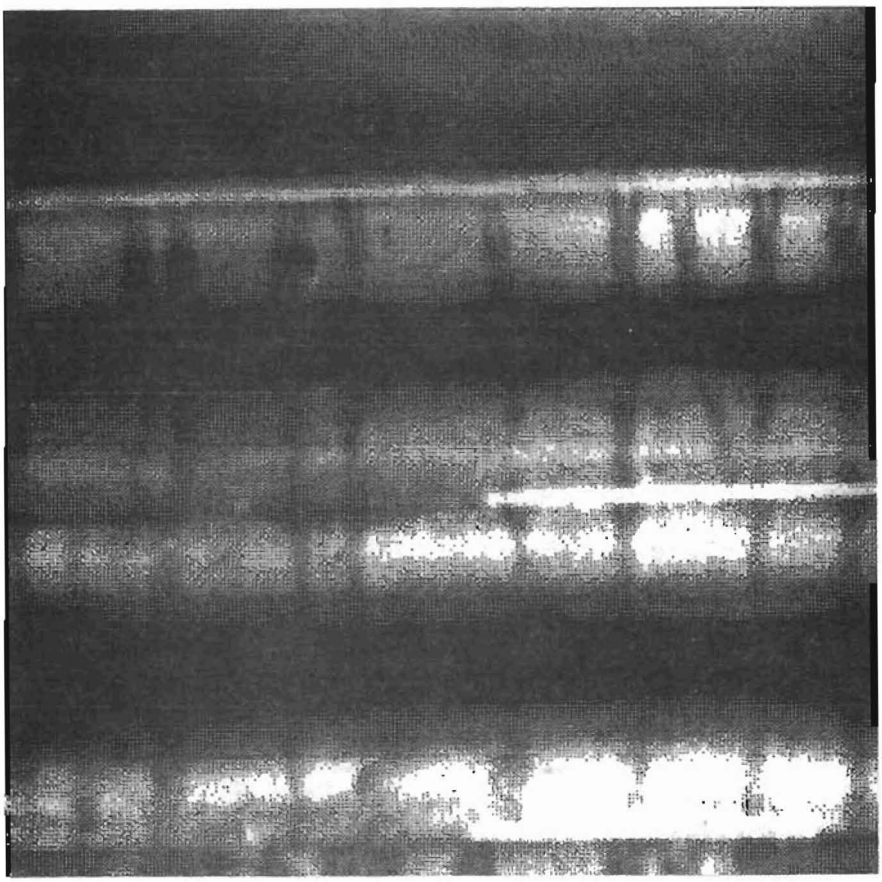

Fig 4.1. Digitized picture of a highway pavement (Hwy 3).

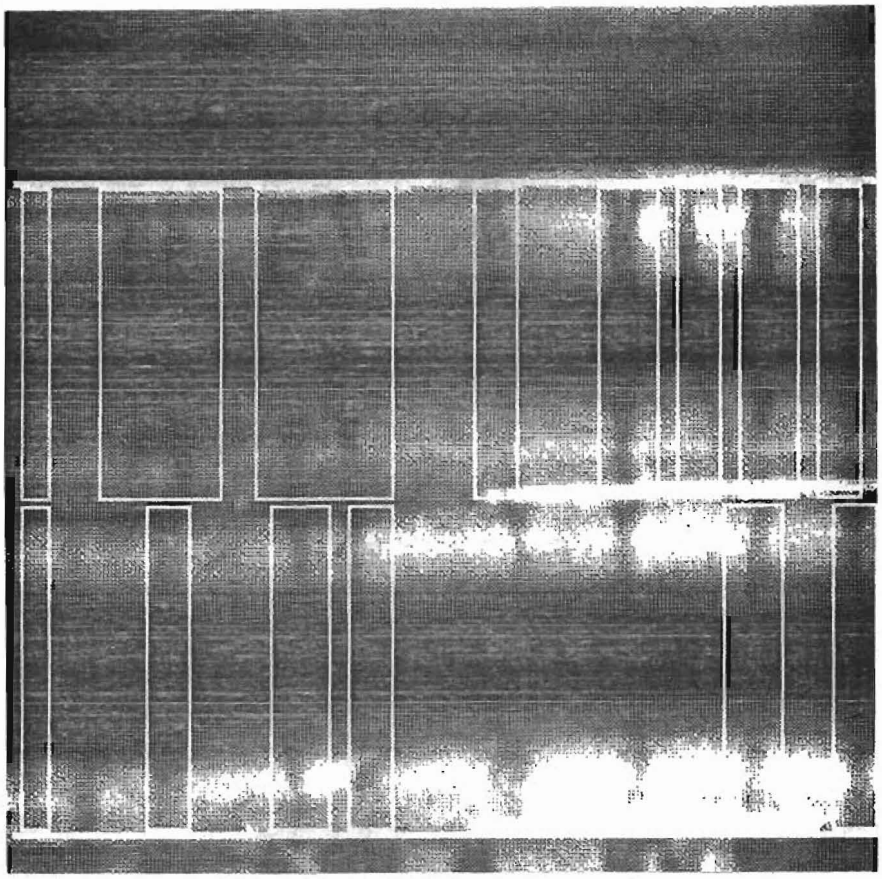

Fig 4.2. Modified picture of Fig 4.1. The regions with a high density of water marks are circled by white frames.

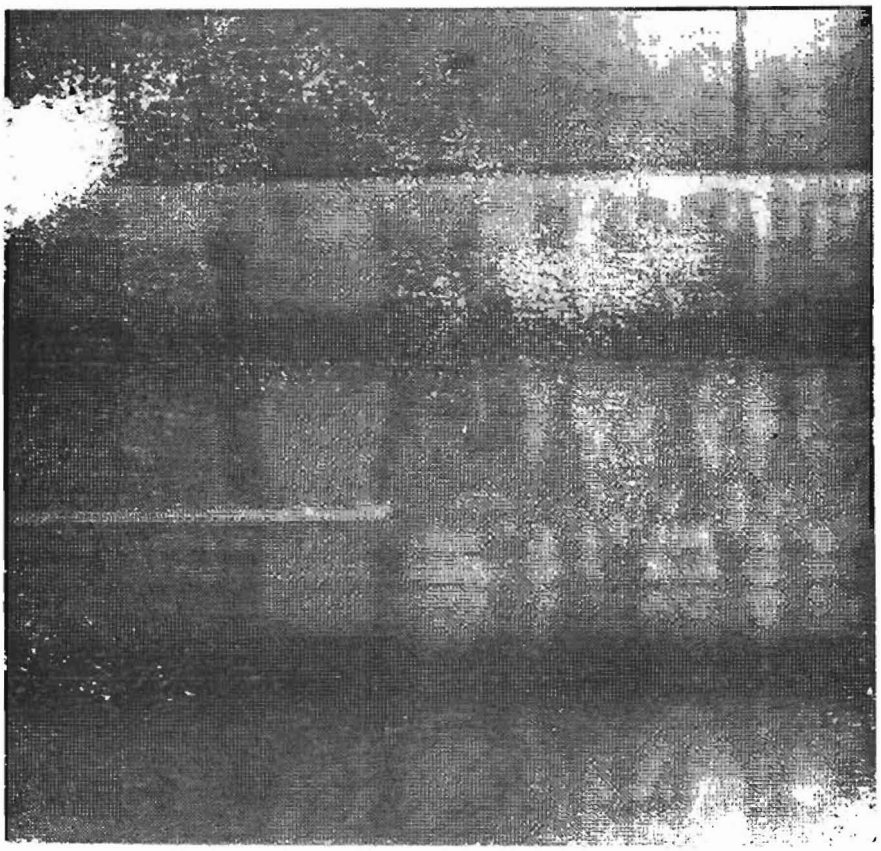

Fig 4.3. Digitized picture of a highway pavement (Hwy 4).

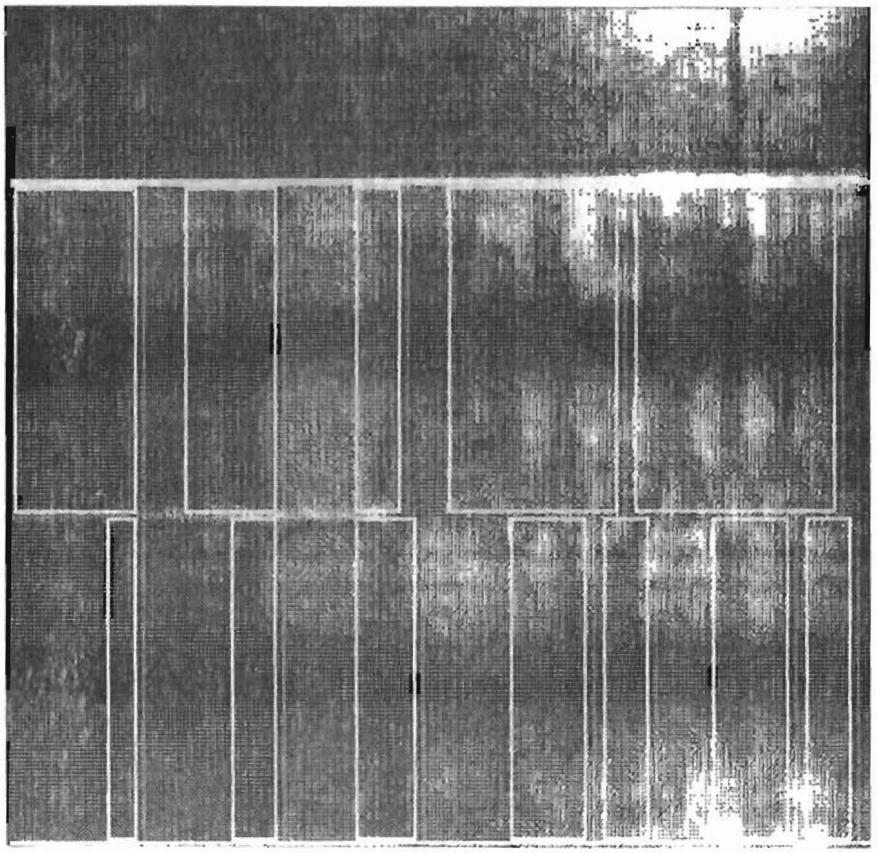

Fig 4.4. Modified picture of Fig 4.3. The regions with a high density of water marks are circled by white frames.

(2) Test the number of edge points on each potential edge line and label it as a "potential boundary" if the number of edge points on it is a local maximum.

(3) Divide the whole lane into subregions separated by potential boundary, and calculate the average intensity for each subregion.

(4) Test the average intensity of each subregion obtained from step 3. A subregion is labelled as a water mark if its average intensity is a local minimum, since the average intensity of the region corresponding to or containing water mark is lower than that of the region that does not correspond to a water mark.

(5) Approximate the location of cracks in the center of each subregion labelled as a water mark in step 4. Calculate the spacing between each pair of cracks, and find the average crack spacing for each lane.

(6) Consider the width for each subregion labelled as a water mark. If the width for one water mark is larger than the average width, there may be more than one crack in "this" water mark. Modify the number of cracks and crack spacings by taking into account "this" water mark.

The results of performing this algorithm on road pictures are depicted in Figs 4.5 through 4.8. In Figs 4.5 and 4.7, the center of each water mark is marked with a white line. In Figs 4.6 and 4.8, each water mark is bounded by a white frame. The resulting center positions and widths of water marks are tabulated in Table 4.1.

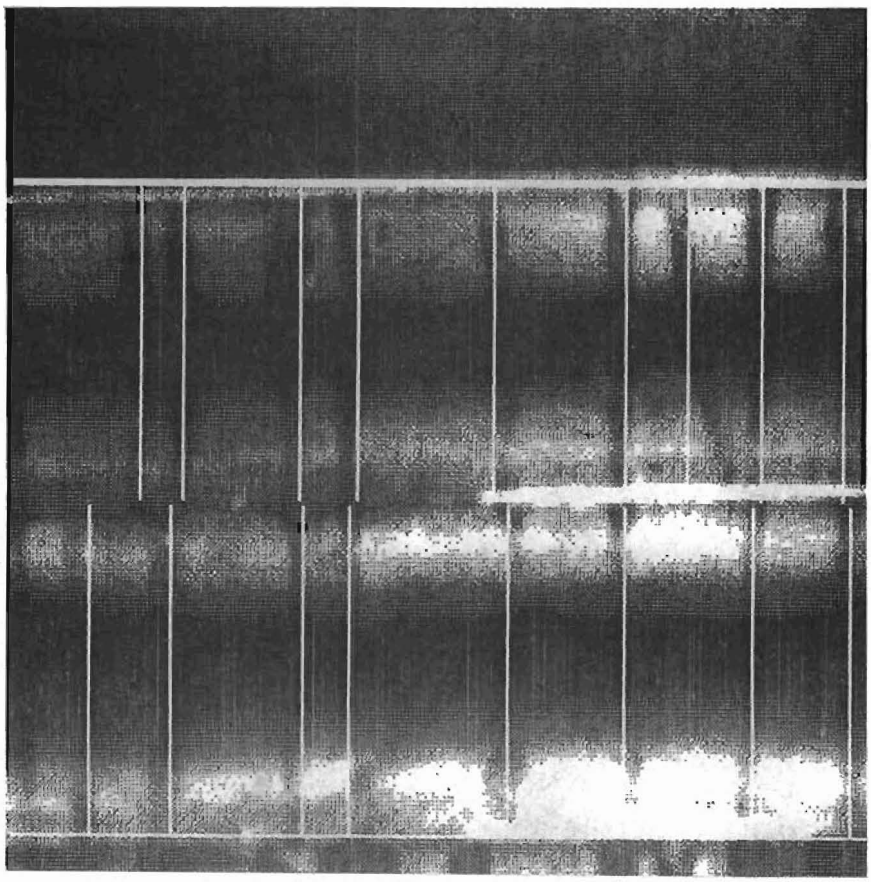

Fig 4.5. Modified picture of Fig 4.1 with white lines indicating the location of cracks.

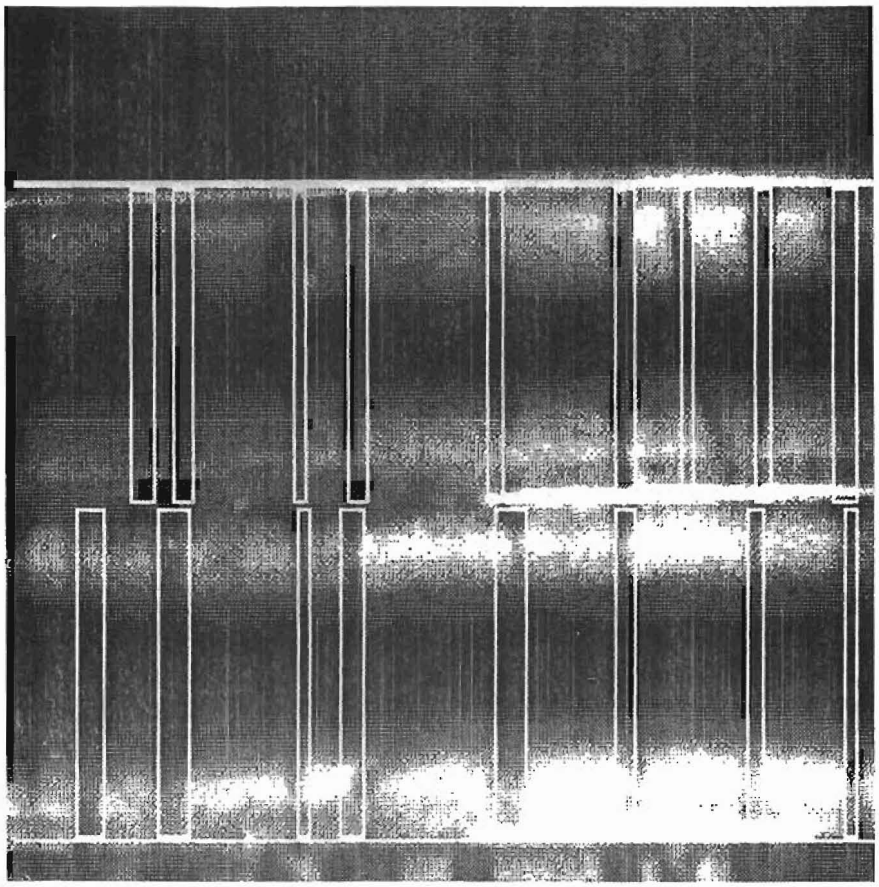

Fig 4.6. Modified picture of Fig 4.1 with white frames indicating water marks.

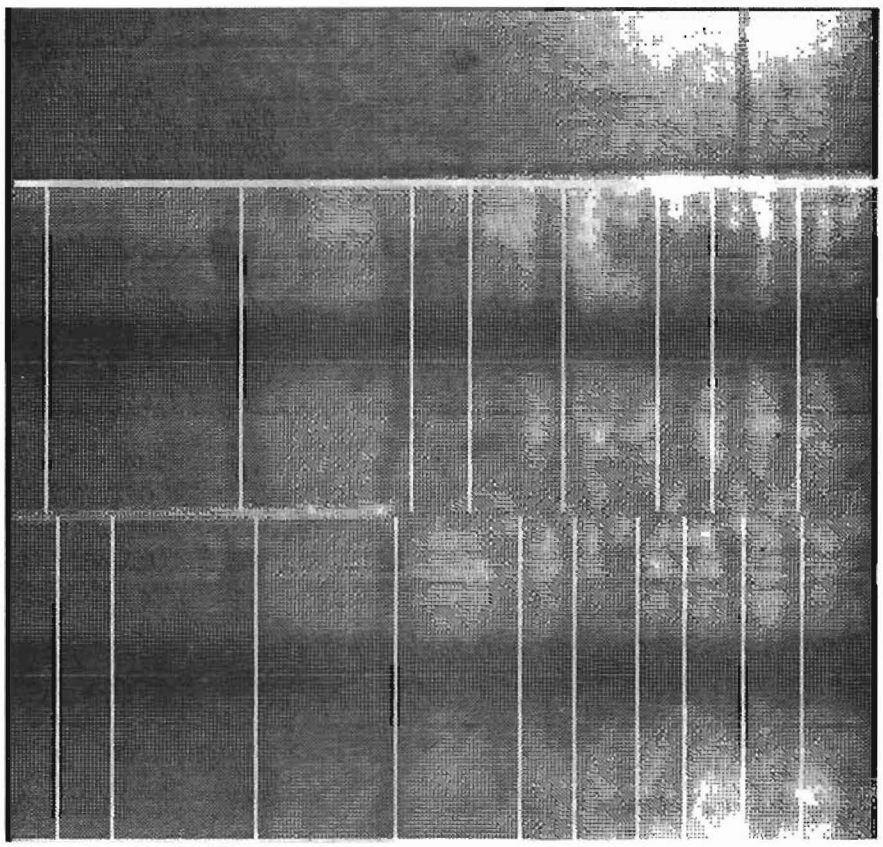

Fig 4.7. Modified picture of Fig 4.3 with white lines indicating the location of cracks.

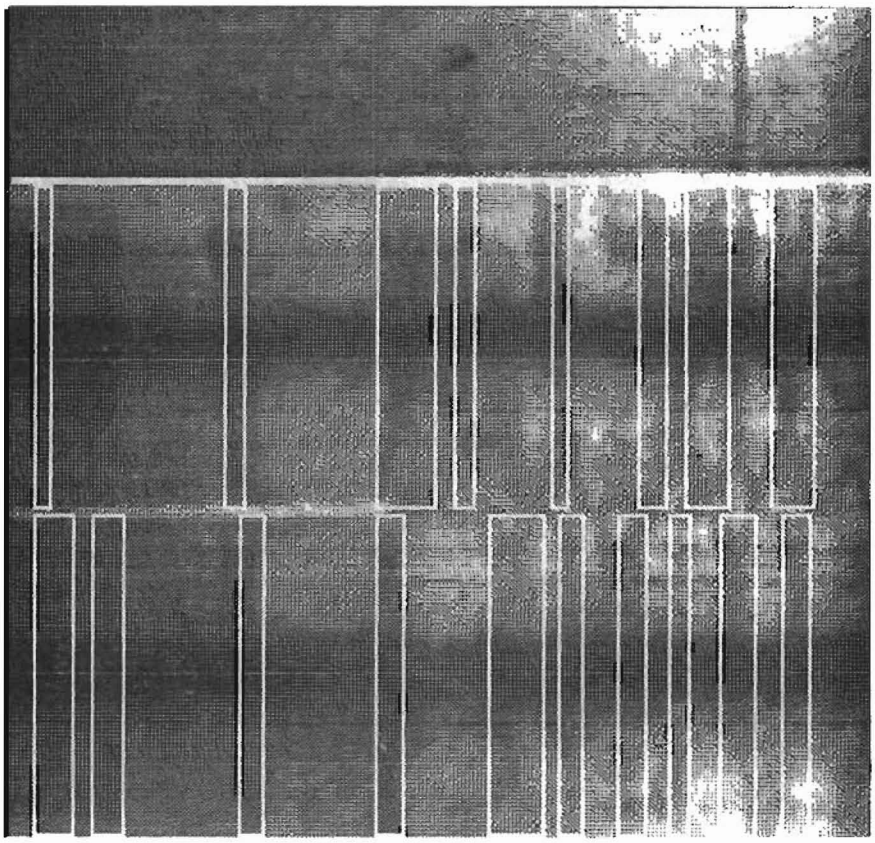

Fig 4.8. Modified picture of Fig 4.3 with white frames indicating water marks.

TABLE 4.1. THE CENTER POSITION AND WIDTH OF WATER MARK

(a) UPPER LANE OF FIG 4.1

| Center position | 37 | 48 | 78 | 93 | 128 | 162 | 178 | 197 | 218 |
|---|---|---|---|---|---|---|---|---|---|
| Width | 6 | 5 | 3 | 5 | 4 | 5 | 3 | 4 | 6 |

Average Width of Water Mark: 4.56 pixels (0.66 ft)

Average Spacing of Cracks : 22.63 pixels (3.27 ft)

Scale : 83 pixels per 12 feet

(b) LOWER LANE OF FIG 4.1

| Center position | 24 | 45 | 79 | 91 | 132 | 162 | 195 | 220 |
|---|---|---|---|---|---|---|---|---|
| Width | 7 | 8 | 3 | 6 | 8 | 5 | 4 | 3 |

Average Width of Water Mark: 5.5 pixels (0.80 ft)

Average Spacing of Cracks : 28.0 pixels (4.04 ft)

Scale : 83 pixels per 12 feet

TABLE 4.1. (continued)

(c) UPPER LANE OF FIG 4.3

| Center position | 12 | 62 | 106 | 121 | 145 | 169 | 183 | 205 |
|---|---|---|---|---|---|---|---|---|
| Width | 4 | 5 | 15 | 5 | 4 | 7 | 11 | 11 |

Average Width of Water Mark: 7.75 pixels (1.11 ft)

Average Spacing of Cracks : 31.86 pixels (4.55 ft)

Modified Crack-Spacing : 27.88 pixels (3.98 ft)

Scale : 84 pixels per 12 feet

(d) LOWER LANE OF FIG 4.3

| Center postion | 15 | 30 | 66 | 102 | 134 | 148 | 164 | 176 | 191 | 206 |
|---|---|---|---|---|---|---|---|---|---|---|
| Width | 10 | 7 | 6 | 7 | 13 | 7 | 7 | 5 | 9 | 7 |

Average Width of Water Mark: 7.70 pixels (1.10 ft)

Average Spacing of Cracks : 21.22 pixels (3.03 ft)

Scale : 84 pixels per 12 feet

# CHAPTER 5. EVALUATION OF ALGORITHMS

## ACCURACY

Accuracy is an important concern in this study. To evaluate the accuracy of this technique, the actual crack spacings were measured directly from the aerial photographs (based on the knowledge that the lane-width of the highway pavement is 12 feet). The actual and estimated crack spacings (with modification) for the road pictures of Figs 4.1 and 4.3 are shown in Table 5.1.

## TIME ESTIMATE

The processing techniques described in this report are executed on a minicomputer PDP-11/34 which is a sequential machine. The time charge for PDP-11/34 in the Advanced Graphic Laboratory (AGL) at the University of Texas at Austin is 30 dollars/hour based on real working time but not on machine CPU time. The total time to process one picture is about 9 minutes of CPU time, distributed as follows:

| | | |
|---|---|---|
| (1) | Picture digitization | 0.5 min |
| (2) | Kirsch operator application | 2.0 min |
| (3) | Non-maxima suppression | 1.0 min |

TABLE 5.1. ACTUAL AND ESTIMATED CRACK SPACINGS FOR FIGS 4.1 AND 4.3

| | Actual | Estimated |
|---|---|---|
| Fig 4.1 (upper) | 3.3 ft | 3.3 ft |
| (lower) | 4.0 ft | 4.0 ft |
| Fig 4.3 (upper) | 3.5 ft | 3.4 ft |
| (lower) | 3.0 ft | 3.0 ft |

| | | |
|---|---|---|
| (4) | Binary picture computation | 0.5 min |
| (5) | Hough transform application | 1.5 min |
| (6) | Road detection | 1.0 min |
| (7) | Locating water marks and cracks | 2.5 min |

Processing is computationally expensive. PDP-11 is a sequential machine and its main memory cannot contain the entire 256 x 256 picture. Thus, the picture must be stored in auxiliary memory and the portion of the picture being processed must be read into main memory. Transferring data between main memory and auxiliary memory takes more time than actual computations in our study. Time to process a digital picture can be drastically reducted using a parallel architecture, such as the Staran Parallel Computer (Ref 17).

# CHAPTER 6. CONCLUSION

In this study, crack spacings for CRC pavements have been estimated with reasonable accuracy using a computer graphic technique. First, the Kirsch operator was applied for gradient computation. The non-maxima suppression procedure was performed on the gradient picture to select those pixels at which the gradient values were local maxima. Thresholding was applied before and after the non-maxima suppression procedure using a low threshold $T_{g_1}$ and a high threshold $T_{g_2}$ for locating water marks and extracting the lines in the direction of the road. Extracting the lines was accomplished using a modified version of the Hough transform, and the direction of the road was determined and the road sections were subsequently located. Potential edge lines are labelled according to the number of edge points (corresponding to water marks) on the potential edge lines. Finally, with the knowledge of potential boundaries, water marks were located, cracks were approximately located in the middle of water marks, and crack spacings were calculated.

In the condition surveys of rigid pavements, particularly CRC pavements, the crack spacing is an essential element. It provides an indicator of the general condition of the pavement. It would be particularly useful in forecasting potential problem areas if historic data were available. As the crack spacing decreases (or the number of cracks per unit length of pavement increases) the condition of the pavement is deteriorating.

Tables 4.1a and 4.1b show that the average crack spacing for the upper lane of Fig 4.1 is 22.63 pixels, or 3.27 feet, and for the lower lane is 28 pixels, or 4.04 feet. Therefore, the pavement condition of the lower lane is better than that of the upper lane. However, based on this evidence only, it cannot be concluded that the pavement of the upper lane is in bad condition. There are other parameters for evaluating pavement condition, such as magnitude of deflections and openings of cracks.

This report does not provide for a complete survey of the condition of the highway pavement, not covering such as deflection, spalling, and patching (Ref 18). The reason is that, with relatively low resolution (for our study), information about the condition of the pavement which can be obtained from the digitized picture is limited. Future research will develop techniques for detecting deflection, spalling, and patches for the evaluation of the condition of highway pavements if pictures of highway pavements with relatively high resolution are available.

The method is expensive, costing about $600.00 per mile for computer time alone. Additionally the difficulty of obtain low level, high resolution aerial photograph of a wetted pavement make the method more costly than ground surveys and it generates less information. When refinement in aerial photography and computer graphics occur, the method may be more applicable. However at the present time the method is not practically applicable to highway pavement evaluation.

REFERENCES


1. Park, R., and T. Pauley, Reinforced Concrete Structures, John Wiley & Sons, New York, 1975.

2. Kirsch, R., "Computer Determination of the Constituent Structure of Biological Images," Computers and Biomedical Research, 4, 3, 1972, p 315-328.

3. Davis, L. S., S. A. Johns and J. K. Aggarwal, "Texture Analysis Using Generalized Co-Occurrence Matrices," IEEE Trans. on Pattern Analysis and Machine Intelligence, Vol 1, PAMI-1, No. 3, July 1979, p 251-259.

4. Duda, R. O., and P. E. Hart, "Use of the Hough Transformation to Detect Lines and Curves in Pictures," Commun. ACM, 15, 1, January 1972, p 11-15.

5. Marr, D., and E. Hildreth, Theory of Edge Detection, MIT AI Laboratory AI Memo No. 518, April 1979.

6. Roberts, L. G., "Machine Perception of Three Dimensional Solids," Optical and Electro-Optical Information Processing, J. T. Tippett, et al., Eds., MIT Press, Cambridge, Mass., 1965, p 159-197.

7. Duda, R. O., and P. E. Hart, Pattern Classification and Scene Analysis, John Wiley & Sons, New York, 1973.

8. Prewitt, J. M. S., "Object Enhancement and Extraction," Picture Processing and Psychopictorics, B. S. Lipkin and A. Rosenfeld, Eds., Academic Press, New York, 1970.

9. Argyle, E., "Techniques for Edge Detection," Proceedings, IEEE, 59,2, February 1971, p 285-287.

10. Macleod, I. D. G., "Comments on 'Techniques for Edge Detection'," Proceedings, IEEE, 60, 3, March 1972, p 344.

11. Rosenfeld, A., M. Thurston, and Y. Lee, "Edge and Curve Detection: Further Experiments," IEEE Trans. on Computers, C-21, 7, July 1971, p 677-715.

12. Pratt, W. K., Digital Image Processing, John Wiley & Sons, New York, 1978.

13. Rosenfeld, A., and A. Dak, Digital Picture Processing, Academic Press, New York, 1976.

14. Hough, P. V. C., "Method and Means for Recognizing Complex Patterns," U. S. Patent 3069654, December 18, 1962.

15. Fennama, C. L., and W. B. Thompson, "Velocity Determination in Scenes Containing Several Moving Objects," Comput. Graphics Image Processing, Vol 9, April 1979, p 301-315.

16. Bajcsy, R., and D. A. Rosenthal, "Visual and Conceptual Focus of Attention," Structured Computer Vision, S. Tanimoto and A. Klinger, Eds., Academic Press, New York, 1980.

17. Rohrbacher, D., and J. L. Potter, "Image Processing with the Staran Parallel Computer," IEEE Computer, Vol 10, No. 8, August 1977, p 54-59.

18. Yoder, E. J., and M. W. Witczak, Principles of Pavement Design, John Wiley & Sons, New York, 1975.